Diffusing-wave spectroscopy in an inhomogeneous object: Local viscoelastic spectra from ultrasound-assisted measurement of correlation decay arising from the ultrasound focal volume

R. Sriram Chandran,[1] Saikat Sarkar,[2] Rajan Kanhirodan,[3] Debasish Roy,[2] and Ram Mohan Vasu[1,*]
[1]*Department of Instrumentation and Applied Physics, Indian Institute of Science, Bangalore-560012, India*
[2]*Department of Civil Engineering, Indian Institute of Science, Bangalore-560012, India*
[3]*Department of Physics, Indian Institute of Science, Bangalore-560012, India*
(Received 2 April 2014; published 8 July 2014)

We demonstrate diffusing-wave spectroscopy (DWS) in a localized region of a viscoelastically inhomogeneous object by measurement of the intensity autocorrelation $[g_2(\tau)]$ that captures only the decay introduced by the temperature-induced Brownian motion in the region. The region is roughly specified by the focal volume of an ultrasound transducer which introduces region specific mechanical vibration owing to insonification. Essential characteristics of the localized non-Markovian dynamics are contained in the decay of the modulation depth $[M(\tau)]$, introduced by the ultrasound forcing in the focal volume selected, on $g_2(\tau)$. The modulation depth $M(\tau_i)$ at any delay time τ_i can be measured by short-time Fourier transform of $g_2(\tau)$ and measurement of the magnitude of the spectrum at the ultrasound drive frequency. By following the established theoretical framework of DWS, we are able to connect the decay in $M(\tau)$ to the mean-squared displacement (MSD) of scattering centers and the MSD to $G^*(\omega)$, the complex viscoelastic spectrum. A two-region composite polyvinyl alcohol phantom with different viscoelastic properties is selected for demonstrating local DWS-based recovery of $G^*(\omega)$ corresponding to these regions from the measured region specific $M(\tau_i)$vsτ_i. The ultrasound-assisted measurement of MSD is verified by simulating, using a generalized Langevin equation (GLE), the dynamics of the particles in the region selected as well as by the usual DWS experiment without the ultrasound. It is shown that whereas the MSD obtained by solving the GLE without the ultrasound forcing agreed with its experimental counterpart covering small and large values of τ, the match was good only in the initial transients in regard to experimental measurements with ultrasound.

DOI: 10.1103/PhysRevE.90.012303 PACS number(s): 83.85.Ei, 87.15.Vv, 83.60.Bc, 87.15.Ya

I. INTRODUCTION

Diffusing-wave spectroscopy (DWS) [1,2] is a means to extend the application of dynamic light scattering (DLS) [3] to multiple scattering thick media enabling the study of thermally induced fluctuations of embedded probe particles. Since photons take circuitous paths involving many scattering events in their traverse through such thick objects, fluctuation in intensity is contributed to by the small-scale mechanical vibration of many scatterers (with displacements of the order of a few angstroms), leading to the study of dynamics at such length scales from the measured decay in intensity correlation. Through this, the DWS provides an experimental tool to explore the microscopic origin of the viscoelastic properties of a number of soft materials such as polymer gels, emulsions, and colloids [4]. Relieving a major restriction to the DLS, wherein the specimen studied has to be thin, the DWS paves the way to successfully employ light scattering methods en route to the study of dynamics in thick turbid objects such as soft tissues. However, the objects studied are almost always homogeneous in dynamics and the decay in intensity correlation $[g_2(\tau)$, τ being the delay time] is used to extract mean-squared displacement (MSD) of scattering centers, from which the space-averaged complex elastic spectrum, pertaining to the entire object, is extracted. In order to bring a specimen with inhomogeneous inclusions (from the dynamics perspective) under the scope of application of the DWS, a tomographic approach, called the diffuse correlation tomography (DCT), has been suggested. Here boundary measurements of $g_2(\tau)$ are used to recover spatially varying dynamics such as particle diffusion coefficient D_B [5,6]. Without resorting to a full-fledged tomographic inversion, there are also attempts to recover inhomogeneous dynamics like flow in capillary tube embedded in a thermally driven turbid medium by analyzing the decay of amplitude autocorrelation $[g_1(\tau)]$ [7,8]. Here location of the capillary and the flow profile are successfully recovered if the depth of the capillary in the background object is within $\sim 11l^*$, where l^* is the transport mean-free path of light [8].

The DCT which can recover both the inhomogeneous optical properties [such as absorption coefficient, $\mu_a(\mathbf{r})$] and dynamics [9] can be considered as an extension of the well-known diffuse optical tomography made popular through its extensive application in medical diagnostic imaging [10]. It has recently been demonstrated that a localized recovery of $\mu_a(\mathbf{r})$ and mechanical properties such as elasticity modulus $[E(\mathbf{r})]$ and density with an improved spatial resolution is possible by bringing in an external perturbation with a focused ultrasound (US) beam. The effect of the US beam on the fluctuations of speckle formed by coherent light transport through the insonified region was first discussed in [11]. This modification known as ultrasound-assisted optical tomography [12–14] has been successfully employed even for quantitative, spatially resolved recovery of both $\mu_a(\mathbf{r})$ and $E(\mathbf{r})$ pertaining to the insonified focal volume [referred to as the region of interest (ROI)]. Even though the effect of the localized mechanical vibration is seen in the measured $g_2(\tau)$ in the boundary as a sinusoidal modulation superimposed, it was not known how to extract the

*Corresponding author: vasu@isu.iisc.ernet.in

decay in the intensity autocorrelation that pertains only to the localized dynamics of the ROI from the perturbed $g_2(\tau)$. In this work we suggest that such a "local" decay is available in $g_2(\tau)$ as the decay of the superimposed modulation depth (M). However, its extraction from M is not quite straightforward, owing to the fact that the stochastic process describing the light amplitude (or intensity) that in turn carries information on the dynamics of particles in the ROI is nonstationary. This happens as the localized dynamics in the ROI, induced by the sinusoidal forcing, is nonstationary. Therefore, a proper statistical description could be through an evolutionary autocorrelation (and an evolutionary power spectrum) of the detected intensity [15]. As described below, we achieve this in a straightforward manner: by computing short-time autocorrelations and finding the power contained in it at the ultrasound drive frequency ω_a. That we need only to extract information at a single frequency in the spectral domain (i.e., correspondent to a zero spectral bandwidth in the evolutionary power spectrum) gives us the freedom to have the slowly evolving power spectrum be computed at a time resolution as high as allowed by the modulation frequency ω_a. The evolutionary power at $\tau = \tau_i$ is computed by Fourier transforming the short-time autocorrelation evaluated around $\tau = \tau_i$ and finding the modulus of the Fourier transform at $\omega = \omega_a$, the drive frequency of the US transducer.

From the decay of $M(\tau)$ with τ we extract visoelastic spectra, pertaining to the ROI, and call this new method "local DWS." A number of advantages hitherto unattainable with the usual DWS can be reaped. As demonstrated experimentally here, using a jelly-like, inhomogeneous polyvinyl alcohol (PVA) phantom, one can extract viscoelastic spectra pertaining to different regions in the object from the experimentally measured decays in $M(\tau)$ with the US focal volume in those regions. In addition, it is conjectured (not demonstrated here, but reserved for a future publication) that the local DWS can detect capillary flow hidden deep within anywhere in a turbid thermally driven object (not restricted to a multiple of l^* from the boundary as in [8]) from the way $M(\tau)$ vs τ decays when the US focal volume intercepts the capillary, and also extract quantitative information on the flow profile. Moreover, by making the ROI small enough by "beating" two US focal volumes at its thinnest waist region, one can, with proper selection of scattering particle density in the ROI, ensure that there is only one scattering event in the ROI. With this, from the measured $M(\tau)$ vs τ, one can extract particle size distribution and viscoelastic properties following the theoretical framework of DLS [3]. Thus DLS can be employed in a large volume turbid object to any selected small ROI within.

A summary of the rest of the paper is as follows: In Sec. II we model the temperature-induced dynamics of the particles in the ROI using a generalized Langevin equation and arrive at their MSD (The dynamics in the presence of external US forcing is considered in the Appendix.). Section III describes the experiments done to gather the modulated $g_2(\tau)$ from a composite PVA phantom with the US focal volume in either of the two regions of the phantom. From $g_2(\tau)$, $M(\tau)$ is found which is used to arrive at the storage and loss modulus spectra. The results are discussed in Sec. IV and our conclusions are set forth in Sec. V.

II. A GENERALIZED LANGEVIN MODEL OF THE DYNAMICS

Here one aims at modeling the dynamics of the particles in the ROI, which is roughly the ultrasound (US) focal volume. These temperature driven particles are subjected to an externally applied sinusoidal forcing, the strength of which is kept "small" and the frequency large enough to meet the sampling frequency requirement for extracting the viscoelastic spectrum. Under this circumstance the dimensionless Péclet number (a measure of the relative strength of the external force on the particle vis-à-vis the thermal forces) is small and therefore the dynamics of scattering particles corresponds essentially to a fractional Brownian motion (fBm) with a "small" deterministic sinusoidal perturbation superimposed [16]. As already indicated, coherent light in its passage through the object, in addition to picking up a phase modulation, suffers a loss of coherence owing to the fBm-type diffusion of particles, which is reflected in the decay of the intensity (or amplitude) autocorrelation of the light scattered from them. The phase modulation is reflected in the autocorrelation as a superimposed almost-sinusoidal modulation. In the experiment described in Sec. III, the decay in this modulation depth is measured and related to the MSD of the particles in the ROI.

The aim of the present Langevin model is limited to verifying the MSD of the Brownian particles in the ROI obtained from the experimentally measured decay in M. Towards this, we first consider a homogeneous viscoelastic object with properties made up of the material of the ROI, subject to an fBm-type subdiffusive motion driven only by temperature, i.e., without the external forcing from the US transducer. Let t_0 denote the initial time so that $\tau = t - t_0$ is the delay time. Since we consistently use $t_0 = 0$, the symbols τ,t are interchangeably used to denote both the delay time and the current time. The fBm-type dynamics of a particle in the ROI, a viscoelastic medium, may be modeled through a GLE [17,18], such that the variance of the particle position increases only sublinearly in time. A typical such particle experiences a history-dependent viscous drag modeled with the help of an integral term dependent on the velocity history $\{\dot{x}(s); 0 < s \leqslant t\}$ of the particle, where t denotes the current time. An important component of this integral term is the memory (friction) kernel $\eta(t-s)$. While for a memoryless frictional kernel, i.e., $\eta(t-s) = 2\eta\delta(t-s)$[$\eta$ is a constant and $\delta(t)$ the Dirac delta function], a purely viscous Stokes friction force is experienced by the particle, a nondecaying frictional kernel $\eta(t-s) = \eta$ induces a quasielastic cage forcing. For a viscoelastic object, such as the polyvinyl alcohol phantom of the present study, one may adopt a power law function $\eta(t-s) = \frac{\eta_\alpha (t-s)^{-\alpha}}{\Gamma(1-\alpha)}$, which may be interpreted as an interpolation across the above two extreme scenarios [19]. Here $\Gamma(\cdot)$ denotes the gamma function and subdiffusive dynamics implies that $0 < \alpha < 1$. Assuming a parabolic potential, the GLE is then given by [16]

$$m\ddot{x}(t) + \int_0^t \eta(t-s)\dot{x}(s)ds + \omega^2 x(t) = \xi(t), \qquad (1a)$$

where m is the particle mass, ω^2 is the stiffness coefficient, and $\eta(t-s)$ is the friction kernel. $\xi(t)$ is a zero-mean Gaussian

stationary stochastic (thermal) forcing function arising from the environment (i.e., the harmonic bath oscillators in the Langevin approach). Moreover, Kubo's second fluctuation-dissipation theorem [20] requires that its autocorrelation is related to the memory kernel via $\langle \xi(t)\xi(s)\rangle = k_B T \eta(|t-s|)$ [21], where k_B is the Boltzmann constant and $T = 298$ K, the room temperature. Alternatively, based on a statistical-mechanical derivation of the above GLE, one may argue that the power spectrum $S(\nu) := 2\int_0^\infty \xi(s)\xi(0)\cos \nu s ds$ of $\xi(t)$ is related to the spectral density $B(\nu) \sim \eta_\alpha \nu^\alpha$ of the bath oscillators via $S(\omega) = 2k_B T B(\omega)/\omega$. The above model of viscoelasticity thus corresponds to the sub-Ohmic bath with $0 < \alpha < 1$, wherein the motion would be strictly subdiffusive only if $\omega^2 = 0$.

The solution $x(t)$ to the GLE (1a) is clearly a non-Markovian stochastic process. However, a reduction of the above form to a higher dimensional system of stochastic differential equations (SDEs), whose solution would be Markovian, is possible [21]. This may be accomplished by first effecting a decomposition of $\xi(t)$ as a sum of independent filtered white noise components, i.e., by writing $\xi(t) = \sum_{j=0}^{N-1} \vartheta_j(t)$, where $\langle \vartheta_j(t)\vartheta_j(s)\rangle = k_B T \exp(-\upsilon_j|t-s|)$. The memory kernel $\eta(t-s)$ then admits the consequent decomposition $\eta(t-s) = \sum_{j=0}^{N-1} \eta_j \exp(-\upsilon_j|t-s|)$. Here $\upsilon_j = \upsilon_0/d^j$ is the inverse autocorrelation time of the jth filtered white noise component, d a dilation parameter, υ_0 the high frequency cutoff of $\xi(t)$, $\eta_j = \frac{\eta_\alpha \upsilon_0}{\Gamma(1-\alpha)d^j} C(d)$ the jth weight in the memory kernel expansion, and $C(d)$ a constant. Note that each filtered white noise component $\vartheta_j(t)$ in the expansion of $\xi(t)$ is a solution to the first-order SDE $d\vartheta_j = -\upsilon_j \vartheta_j dt + \sqrt{2\eta_j \upsilon_j k_B T} dW_j(t)$, where $\{W_j(t)\}$ is a family of N-independent standard Brownian noise processes, $\langle W_i(t)W_j(s)\rangle = \delta_{ij}\delta(t-s)$. This yields the following $(N+2)$ dimensional system of SDEs as a Markovian representation of the GLE:

$$dx(t) = v(t)dt, \tag{1b}$$

$$dv(t) = (-\omega^2/m)x dt + (1/m)\sum_{i=0}^{N-1} u_j(t)dt, \tag{1c}$$

$$du_j(t) = [-\eta_j \upsilon_j - \upsilon_j u_j(t)]dt + \sqrt{2\upsilon_j \eta_j k_B T} dW_j(t). \tag{1d}$$

In the presence of an externally applied sinusoidal forcing term with frequency ω_f and amplitude A, Eq. (1c) may be modified as

$$dv(t) = (-\omega^2/m)x(t)dt + (A/m)\sin(\omega_f t)dt + (1/m)\sum_{i=0}^{N-1} u_j(t)dt. \tag{1e}$$

Denoting the solution vector as $\mathbf{X}_t = \{x_t, v_t, u_1, \ldots, u_{16}\}^T$ and noting the linearity of the vector field, one may formally write the general solution to the GLE as

$$\mathbf{X}_t = \mathbf{\Phi}_t \mathbf{X}_0 + \mathbf{\Phi}_t \int_0^t \mathbf{\Phi}_s^{-1}\mathbf{F}_s ds + \mathbf{\Phi}_t \int_0^t \mathbf{\Phi}_s^{-1}\mathbf{H}_s d\mathbf{W}_s.$$

Here $\mathbf{\Phi}_t$ is the fundamental solution matrix (FSM), $\mathbf{F}_t$ the deterministic force vector (containing the sinusoidal forcing term as the only nonzero entry), $\mathbf{H}_t$ the diffusion coefficient matrix, and $\mathbf{W}_t$ a suitably zero-padded vector of pure Brownian components.

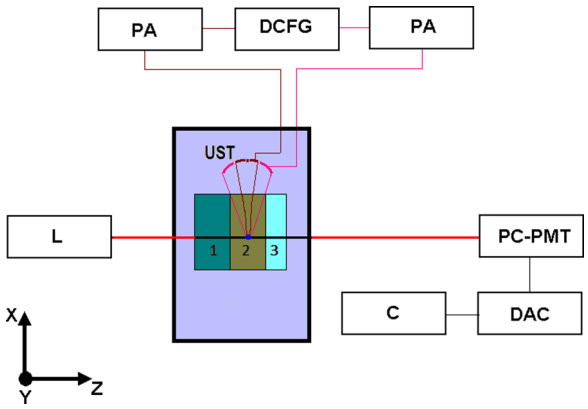

FIG. 1. (Color online) Light emitted from laser source L, illuminates the ROI insonified by confocal ultrasound transducer (UST). The scattered intensity of the light is detected by the detector (PC-PMT) and is given to the correlator DAC and then to a computer C. The UST is driven by power amplifier (PA) that takes input from a dual-channel function generator (DCFG). The sample consists of two slices of PVA, of different storage modulus values, 11 kPa (1) and 23kPa (2), and an ergodic medium (3).

For the GLE (1a) without the sinusoidal forcing, the typical numerical values of the parameters used in the numerical simulations are $\alpha = 0.5$ and $\upsilon_0 = 10^3$ for $d = 2$; $N = 64$ with $C(2) = 0.389$, corresponding to region 1 of the composite phantom used in the experiments described in Sec. III; and $\alpha = 0.5$, $\upsilon_0 = 10^3$, $d = 10$, and $N = 16$ with $C(16) = 1.3$ for region 2 (see the setup in Fig. 1). The set $\{u_j(t)\}_{i=0}^{N-1}$ contains only dummy variables and does not represent any physical quantity. $\{u_j(0)\}$ are independently sampled from a Gaussian distribution with variance $k_B T \eta_j$. A stochastic Heun scheme is used to integrate the coupled SDEs in Eqs. (1b)–(1d) to generate an ensemble of paths within a Monte Carlo setup and thus compute the sample estimate $\langle x(t)^2\rangle$, from which the sample approximation to the MSD $\langle \delta x(t)^2\rangle := \langle x(t)^2\rangle - \langle x(0)^2\rangle$ is retrievable. Note, however, that in the local DWS the US force introduces a perturbation driving the system (the particles in the ROI and the bath oscillators) away from thermal equilibrium. The numerical simulations are carried out with $\alpha = 0.5$ and ω computed using the experimentally measured shear modulus values of the PVA phantoms, the objects used in the experiments described in Sec. III. The results of simulations are given in Sec. III along with their experimental counterparts.

An attempt at direct numerical simulation of the sinusoidally forced GLE [with Eq. (1c) replaced by Eq. (1e)] within a Monte Carlo framework, however, faces difficulties in a high sensitivity of the simulated paths to the choice of Δt, the time step size. Specifically, for $d = 10$ and $N = 16$, the FSM $\mathbf{\Phi}_t$ could be severely ill-conditioned given that the parameters υ_j, η_j go from large to very small as j increases. In other words, for large j, the drift (and even the diffusion) terms in the SDEs for $u_j(t)$ will be negligibly small. Thus, during numerical integration, the error in computing the drift term containing the

deterministic forcing vector $\mathbf{F}_t$ could be substantial, especially so for relatively large $\omega_f \gg \omega$. This is actually the case for the PVA phantom used in the experiments here, when ω_f is of the order of 1 kHz. In addition, as the forcing amplitude A becomes larger, a possible coupling of the dynamical system parameters [e.g., $\eta(t-s)$ and ω^2] with the forcing term could render Kubo's second fluctuation-dissipation theorem untenable and even the present model questionable.

Given the complexities involved in numerically simulating the response of the sinusoidally forced GLE in the transient regime, an alternative approach based on a change of measures is outlined in the Appendix, wherein an integral expression for the MSD is analytically derived [see Eq. (A14)]. As indicated during the derivation, an advantage of this approach is that any modeling errors, such as those in converting the GLE from its non-Markovian to Markovian form, are accounted for in a weak stochastic sense. Of specific interest is the last term on the right-hand side of Eq. (A14) that describes the contribution of the external forcing to the MSD. Since this term, which is a time integral, has a strictly positive integrand, it constitutes a monotonically increasing function in t. However, for small t, because of the presence of an A^2 term, its contribution is small, and the early transient of MSD follows the one corresponding to the nonforced case. Indeed, the contribution of this term becomes significant only when t is sufficiently large, i.e., $t \approx O[(1/A^2)]$. Assuming that, for t large enough, the MSD attains a plateau, this would correspond to a steady state of the evolution equation (A14) such that $\pi_t(x^2) = \pi_{t+\Gamma}(x^2)$, where $\Gamma \simeq \pi/\omega_f$. From the form of Eq. (A14) and its derivation in the Appendix, it is clear that the present plateau is of higher magnitude compared to that obtained from the GLE without the external forcing.

It is seen from the analysis above that the introduction of the ultrasound local forcing has not influenced the extraction of MSD except for large values of t when it attains a steady state. Since we use the transients in MSD for the computation of the viscoelastic spectra, the extracted spectrum by the "local" DWS truly represents its average in the ultrasound focal volume, and is unaffected by the introduction of the eternal force.

III. EXPERIMENTS

We now proceed to experimentally demonstrate our claim that the decay of $M(\tau)$ with respect to τ indeed is caused by the Brownian motion of particles belonging to the ROI. The object used in the experiments is a composite PVA phantom consisting of two rectangular slabs of dimensions 30 mm $\times$ 50 mm $\times$ 8 mm each sandwiched. One is of storage modulus 11 kPa and the other 23 kPa (the corresponding viscous moduli are found to be 2.5 and 4.4 kPa, respectively). The PVA gel does not exhibit ergodic behavior, and therefore the time average $\langle E(\mathbf{r},t)E^*(\mathbf{r},t+\tau)\rangle$ measured cannot be equated to the ensemble average $G(\mathbf{r},\tau)$. In order to restore ergodicity to the medium and thus enable the use of standard theoretical framework to compute complex moduli spectra, we sandwich an ergodic medium (a cuvette with polystyrene spheres of diameter 2 μm and particle density 1.05 g/cc) behind the composite PVA object. Because of the continual random motion of the scattering centers an average of the amplitude autocorrelation across the ensemble is ensured for detection over a finite length of time.

The experimental setup is shown in Fig. 1. The composite PVA phantom (a slab consisting of two sandwiched blocks as described earlier) together with the cuvette is illuminated by the unexpanded beam of light from a He-Ne laser (HRR170, Thorlabs). A confocal ultrasound transducer (UST) mounted on an x-y translation stage provides a focused US beam, whose focal volume can be adjusted to fall fully within either the first or the second block of the composite slab. The axis of the transducer is aligned carefully to be perpendicular to the direction of the light beam. The beam itself is adjusted to intercept the object in the middle region of the US focal volume, which is found to be approximately hyperboloidal. For acoustic impedance matching, the phantom and UST are kept immersed in a water bath.

A single-mode fiber is carefully aligned using a micropositioner to capture a single speckle maximum in the pattern that is available in the light exit plane. Since the signal-to-noise ratio (SNR) in the captured intensity for the signal component, which is the sinusoidal oscillation introduced by the US forcing in the ROI, is usually poor, the alignment of the fiber to maximize SNR is quite critical towards the success of the experiment. The light which is captured by the fiber is delivered to a photon-counting photomultiplier tube (PMT) (Hamamatsu, H7360-03) [22]. The resulting photon current in time (proportional to the light intensity) is converted to a voltage signal and stored in a computer. In a standard DWS experiment, the intensity is autocorrelated via a hardwired autocorrelator, using the so-called multi-τ scheme to compute $g_2(\tau)$ over a large spread in τ, the delay (decay) time, which could be several orders of magnitude (typically from microseconds to tens of seconds) [23,24]. In this scheme the spacing in τ is (quasi) logarithmic which helps to encompass a delay time spanning several decades. However, in our experiments, our objective is to capture (the decay in) the modulation depth which necessitates uniform sampling of intensity beyond the Nyquist rate which in this case is set by the US frequency. Therefore we abandon the multi-τ scheme for the so-called "photon mode" which helps us acquire just the intensity data at any (uniform) rate, bound on the lower end by 16.7 ns, which is the minimum delay interval of the digital autocorrelator used (DAC, Flex 021d, from www.correlator.com, Bridgewater NJ 08807). The acquired intensity data, acquired over an appropriately small time window is autocorrelated using a MATLAB 1-d autocorrelation routine [24]. (The width of the window should be large enough to contain a few periods of the superimposed sinusoidal modulation on $g_2(\tau)$; the modulation frequency is chosen so that it is larger than the Nyquist frequency required to recover the largest frequency of interest in the viscoelastic spectrum of the object being investigated.) In order to reduce the required sampling rate to reasonable values and ensure shear-dominated vibration in the ROI, we have employed a confocal dual-beam UST working at 1MHz and 1.001 MHz producing a beat-frequency forcing in the ROI at 1 kHz. With this frequency the sampling rate at which $g_2(\tau)$ is sampled should only be larger than 2 kHz.

As mentioned earlier, the ergodic medium used is a 4% solution of polystyrene beads (of average diameter 2 μm) in

glycerol ($l^* \simeq 737\ \mu$m from Mie theory [25]). The "double cell" consisting of the phantom and the cuvette shows forth an ergodic behavior. The thickness of the phantom composite and the suspension (L_i, $i = 1,2$, respectively) and their transport mean-free paths l_i^* ($i = 1,2$) are selected such that their optical densities are $L_i/l_i^* = 4$ and 2, respectively, for $i = 1$ and 2. A multiplication rule for the double cell [26], which can be applied to relate the $g_1(\tau)$ of the sandwiched ergodic medium to the individual $g_1(\tau)$'s of the PVA composite and the cuvette, gives us the relation [27,28]

$$g_1(\tau, L_1 L_2) = g_1(\tau, L_1) g_1(\tau, L_2). \tag{2}$$

Here, $g_1(\tau, L_1 L_2)$, $g_1(\tau, L_1)$, and $g_1(\tau, L_2)$ are the normalized field autocorrelations of the double cell, composite PVA gel, and the ergodic medium, respectively.

The specific details of the data gathered through the experiment are given below. First the intensity fluctuation with ergodic medium alone is collected at uniform samples of delay time and stored, and then similar data from the double cell formed between the composite PVA phantom and the cuvette containing the ergodic medium. Two sets of data are collected for the composite phantom: (i) the first corresponds to the US focal volume being centered at the 23 kPa slab and (ii) when it is at the 11 kPa slab. From these intensity data sets $g_2(\tau)$'s for the three cases, namely, pertaining to the ergodic medium, and the composite slabs with US in the 23 and 11 kPa slabs, are computed using the MATLAB autocorrelation routine. The modulus of the normalized amplitude autocorrelation is obtained from $g_2(\tau)$ using the Siegert relation which is $g_2(\tau) = 1 + f|g_1(\tau)|$. The coupling constant f is evaluated from the measured $g_2(\tau)$ at $\tau = 0$ (corresponding to one of the data sets) using $g_2(0) = 1 + f$ [29]. Through the use of a multiplication rule we have extracted $g_1(\tau)$'s corresponding to the composite object, which are shown in Fig. 2. From the $g_1(\tau)$'s of Fig. 2 we have extracted decay of the superimposed sinusoidal modulation with delay time using short-time Fourier transform. We have used a rectangular time window of length 4 ms and slid the window over the entire range of $g_1(\tau)$. The Fourier transform magnitude at $\omega_a = 1$ kHz, the beat frequency of the superimposed US beams in the ROI [$M(\tau)$] is plotted against τ and the plots are shown in Fig. 3 corresponding to

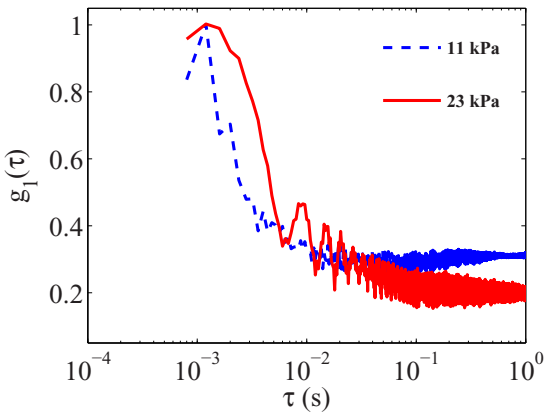

FIG. 2. (Color online) Normalized field autocorrelation plots for individual phantoms, with US in 11 kPa (- - -) and 23kPa (—), extracted using the multiplication rule [Eq. (2)].

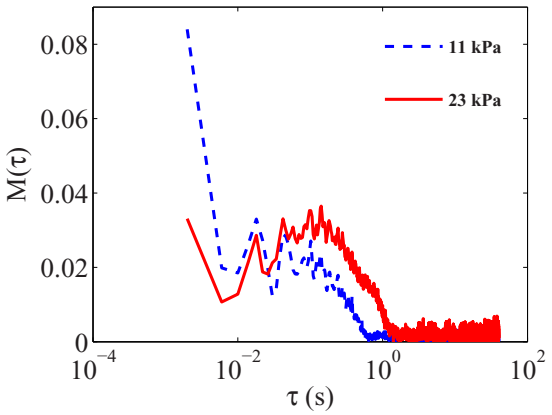

FIG. 3. (Color online) Modulation depth decay when the ROI is in either of the two regions in the composite phantom.

the two cases of the US focal volume in the two regions of the phantom. Since the US beat frequency which modulates $g_1(\tau)$ is 1 kHz, the sampling time used inside the time window to extract $M(\tau)$ should be at least 0.5 ms. On the other hand, a sample time of less than 2.0 ms is pointless in $M(\tau)$, for the 1 kHz US modulation "samples" $g_1(\tau)$. Owing to this and also because of the logarithmic scale used for τ in Fig. 3, $M(\tau)$ corresponding to relatively small values of τ appears noisy and broken. However, the decay of $M(\tau)$ from $\tau = 10^{-1}$ s to 1 s which is properly brought out, is clearly seen to depend on where the US focal volume is in the phantom.

The vibration in the US focal volume, induced by the sinusoidal forcing, causes the modulation we have observed on the measured $g_2(\tau)$. Because of temperature-induced fluctuations of the scattering centers in the ROI, the strength of the cross-correlation term (i.e., the modulation depth) detected in the speckle intensity, whose genesis is the sinusoidal oscillation generated at the ROI, decays with τ. Neglecting optical absorption in the ROI, $M(\tau)$ is related to $\langle \delta x^2(\tau) \rangle$, the mean-squared displacement of scattering centers undergoing Brownian motion through [30]

$$M(\tau) = \exp\left[-\left(\frac{L}{l^*} \right)^2 k_0^2 \langle \delta x^2 \rangle \right]. \tag{3}$$

Here L is the thickness of the US focal volume where the induced forcing is nonzero. From $\langle \delta x^2(\tau) \rangle$ the frequency-dependent complex modulus of elasticity $G^*(\omega)$ is determined using the established procedure used in DWS. The method uses the following relations [31]:

$$G^*(\omega) = \frac{k_B T}{\pi \varsigma i \omega F\{\langle \delta x^2(\tau) \rangle\}}, \tag{4}$$

where T is the temperature in Kelvin, ς is the mean scattering center size, and F represents the operator for Fourier transformation. The storage and loss moduli spectra $G'(\omega)$ and $G''(\omega)$ are computed using [32,33]

$$G'(\omega) = G(\omega)\{1/[1 + \beta'(\omega)]\} \times \cos\left[\frac{\pi \alpha'(\omega)}{2} - \beta'(\omega)\alpha'(\omega)\left(\frac{\pi}{2} - 1 \right) \right], \tag{5}$$

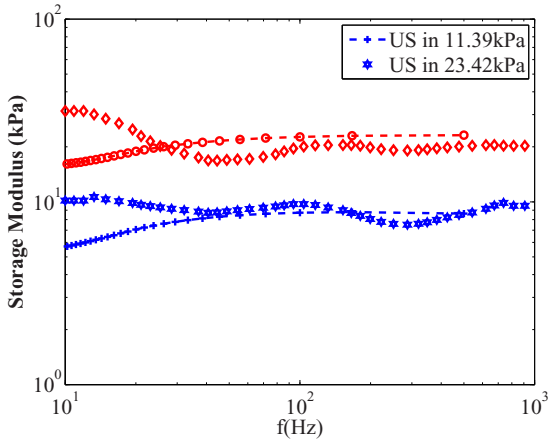

FIG. 4. (Color online) Comparison of storage moduli spectra obtained by localized ultrasound-assisted DWS from the measured $M(\tau)$ decay (-+-+- when the US forcing is in the 11 kPa block and -○-○- when the US forcing is in the 23 kPa block) with those obtained from the usual DWS-based measurement of $g_2(\tau)$ decay for individual homogeneous phantoms (* * for the 11 kPa block and ◊ ◊ for the 23 kPa block).

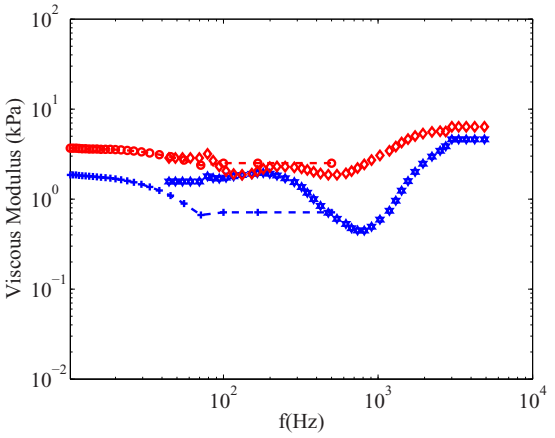

FIG. 5. (Color online) Comparison of loss moduli spectra obtained by localized ultrasound-assisted DWS from the measured $M(\tau)$ decay (-+-+- when the US forcing is in the 11 kPa block and -○-○- when the US forcing is in the 23 kPa block) with those obtained from the usual DWS measurement of $g_2(\tau)$ decay with homogeneous phantoms (* * for the 11 kPa block and ◊ ◊ for the 23 kPa block).

$$G''(\omega) = G(\omega)\{1/[1+\beta'(\omega)]\} \times \sin\left\{\frac{\pi\alpha'(\omega)}{2} - \beta'(\omega)[1-\alpha'(\omega)]\left(\frac{\pi}{2}-1\right)\right\}, \quad (6)$$

where

$$G(\omega) = \frac{k_B T}{\pi\varsigma\langle\delta x^2\left(\frac{1}{\omega}\right)\rangle\Gamma[1+\alpha(\omega)][1+\beta(\omega)/2]}, \quad (7)$$

which is the frequency-dependent elastic modulus. Here $\alpha(\omega)$ and $\beta(\omega)$ represent the first- and second-order logarithmic time derivatives of the MSD data. $\langle\delta x^2(1/\omega)\rangle$ gives the magnitude of $\langle\delta x^2(\tau)\rangle$ evaluated at $\tau = 1/\omega$. Moreover, Γ denotes the γ function, $\alpha'(\omega)$ and $\beta'(\omega)$ give the first- and second-order logarithmic derivatives of $G(\omega)$, and ς is the radius of a typical scattering particle. A second-order polynomial fit using a sliding Gaussian window [32,33] is used to smooth the MSD data and to obtain $\alpha(\omega)$ and $\beta(\omega)$. The values used are 6.6 and 5 (nm) for the storage modulus values of 11 and 23 kPa, respectively [34].

The plots of $G'(\omega)$ and $G''(\omega)$ against ω are shown in Figs. 4 and 5, respectively. For comparison $G'(\omega)$ and $G''(\omega)$ obtained using the standard DWS experiment done on individual samples are also shown in Figs. 4 and 5. The match in $G'(\omega)$ values obtained using the two methods are seen to be quite good, whereas there is some discrepancy in regard to the $G''(\omega)$ plots. This lack of fidelity is owing to the inherent uncertainty of the DWS scheme (with and without the US beam) in measuring the viscous part of the modulus spectrum.

IV. RESULTS AND DISCUSSION

In Figs. 6 and 7 are given the comparison of MSD with the delay time, both computed using the procedure of Sec. II, with those from experiments. The validity of our claim that the decay in correlation in the scattered light introduced by the (fractional) Brownian dynamics in the ROI is indeed contained in the decay in M is verified by the match of the MSD obtained from it with those from simulation and the usual DWS on homogenous phantoms. Whereas the simulation results match more closely with those from the homogenous phantoms, it is not precisely so for the US-assisted results, particularly for large time delays when the MSD reaches a plateau. The input US energy to the ROI, especially when the acoustic absorption cannot be neglected, upsets the thermal equilibrium therein. Because of heat dissipation to the environment, the ROI gradually attains a thermal equilibrium with an elevated temperature. This rise in temperature is reflected in the larger MSD plateau the US-assisted measurements attain in both Figs. 6 and 7. A model to account for the US-induced

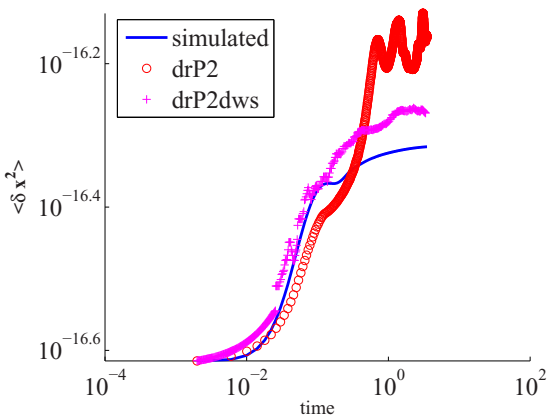

FIG. 6. (Color online) The MSD vs τ graphs, simulated using Eqs. (1b)–(1d) compared with those from experimentally measured autocorrelation with US modulation (circles, drP2) and without (+ symbols, drP2dws), for region 2 in the composite phantom with shear modulus of 23 kPa.

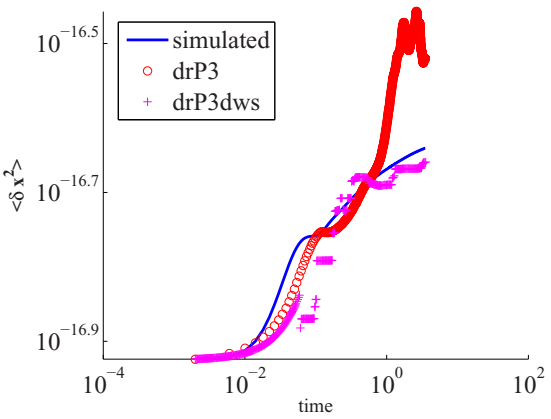

FIG. 7. (Color online) Same as Fig. 6 done for region 1 of the composite phantom with shear modulus of 11 kPa.

(i.e., externally introduced) loss of thermal balance, which would probably need to augment the stiffness term $\omega^2 x(t)$ with a multiplicative noise leading to a time-dependent perturbation to the parabolic potential, which is discussed in a similar context in [17,35], is beyond the scope of the current work. However, as verified in the figures, the effect of such perturbation does not affect, in any significant way, the behavior of MSD in the early transients from which we extract the viscoelastic parameters.

We have also arrived at an analytical expression for the weak solution (i.e., the set of statistical moments) to the GLE, taking into account the US forcing. Though an attempt at direct numerical simulation to the GLE, including the sinusoidal forcing, faces difficulties, it is clear from the analytical expression that the MSD follows its counterpart without forcing (and also the experimental values) in the early time transients, and settles at a higher plateau for large t owing to the influence of the US forcing amplitude. Since we extract the viscoelastic spectrum from the slope of the MSD vs t transients, it is clear that US mediated local extraction of the spectrum is unaffected by the introduction of US perturbation, as long as its amplitude is small enough.

We reiterate that the decay of M shown in Fig. 3, in the time window where it can be delineated, is seen to be different for the two cases of the ROI in the two regions of the phantom. The storage and loss moduli obtained using the new method, and shown in Figs. 4 and 5, seem to reasonably agree with those obtained through the traditional DWS experiments. We also note that the viscoelastic spectra obtained with the new method are reliable only below 500 Hz, since 1 kHz is the sampling frequency used.

V. CONCLUSIONS

An ultrasound-assisted localized recovery of $G'(\omega)$ and $G''(\omega)$, pertaining to the regions identified by the US focal volume, is demonstrated from the measured decay in intensity autocorrelation of diffuse photons. This decay which appears as modulation decay in the detected speckle intensity is measured from $g_2(\tau)$. Towards this, the evolutionary power spectrum of $g_1(\tau)$ is measured at the US frequency. In modeling the temperature-induced viscoelastic dynamics within the ROI, an appropriate form of the generalized Langevin equation is made use of (without accounting for the US-induced forcing term). Whereas the theoretically computed MSD from this model is seen to match the one experimentally arrived at from a homogeneous phantom through the usual DWS quite well, this match is good only for early time delays when the experimental measurement is from $M(\tau)$, the modulation decay. The reason for the mismatch for larger time delays may be that either (1) the energy from the US upsets the thermal equilibrium of the ROI, and makes the particles therein to either settle at a higher plateau of MSD or even escape the cage force or (2) there is a mixing of the effect of external periodic force with that of the temperature-induced random force so that the large-time behavior of the MSD is influenced by it. Among these, the first can be done away with by making the external force small enough. In the present work, on the basis of a change of measures, an integrodifferential equation describing the time evolution of the MSD is derived, while accounting for the possible modeling or approximation errors. Through this, it is shown that the overall MSD has a contribution from the external forcing that assumes significance only for large values of time. However, for arriving at the viscoelastic spectra, it suffices to use only the early transients. Consequently, the local $G'(\omega)$ and $G''(\omega)$ measured agreed well with independent measurements using the standard DWS on phantoms with homogeneous properties.

APPENDIX

The aim here is to derive, based on a change of measures, the evolution equations for the statistical moments, e.g., the MSD, of the response variables [such as $x(t), v(t)$ and $u_j(t)$] appearing in a state-space representation of the GLE that includes the sinusoidal forcing term. Other than the novelty of the approach in the context of solutions to GLEs, it offers the added advantage of accounting for possible modeling errors in the weak sense.

Under a complete probability space, with a measure P, the GLE under a sinusoidal forcing may be written as

$$m\ddot{x}(t) + \int_0^t \eta(t-s)\dot{x}(s)ds + \omega^2 x(t) = \xi(t) + A\,\sin(\omega_f t), \tag{A1a}$$

where A is the amplitude of forcing and ω_f is the forcing frequency. A Markovian representation of the GLE may be given as below:

$$dx(t) = v(t)dt, \tag{A1b}$$

$$dv(t) = (-\omega^2/m)x(t)dt + (A/m)\sin(\omega_f t)dt + (1/m)\sum_{i=0}^{N-1} u_j(t)dt, \tag{A1c}$$

$$du_j(t) = [-\eta_j \upsilon_j - \upsilon_j u_j(t)]dt + \sqrt{2\upsilon_j \eta_j k_B T}\,dW_j(t). \tag{A1d}$$

Note that the P-Brownian motion $\mathbf{W} = \{W_0, \ldots, W_{N-1}\}^*$ is also taken into account for the modeling errors, e.g., those

arising from such sources as the approximation of the memory kernel $\eta(t-s)$. Let $\mathcal{F}_t^W$ denote the current filtration (i.e., the statistical information in the form of collections of σ algebras generated up to the current time t) by $\mathbf{W}_s, s \leqslant t$. As a first step towards investigating the influence of forcing on the MSD, Eqs. (A1b)–(A1d) are recast as

$$dx(t) = v(t)dt, \tag{A2a}$$

$$dv(t) = (-\omega^2/m)x(t)dt + (1/m)\sum_{i=0}^{N-1}\tilde{u}_j(t)dt, \tag{A2b}$$

$$d\tilde{u}_j(t) = [-\eta_j v_j - v_j\tilde{u}_j(t)]dt + \sqrt{2v_j\eta_j k_B T}\,dW_j(t) + \frac{A\omega_f}{N}\cos(\omega_f t)dt + \frac{v_j A}{N}\sin(\omega_f t)dt, \tag{A2c}$$

where

$$\tilde{u}_j(t) := u_j(t) + \frac{A}{N}\sin(\omega_f t), \quad j = 0,...,N-1.$$

Interestingly the drift due to forcing may be removed under a new measure, say Q. Hence, under Q, Eqs. (A2a)–(A2c) may be modified as

$$dx(t) = v(t)dt, \tag{A3a}$$

$$dv(t) = (-\omega^2/m)x(t)dt + (1/m)\sum_{i=0}^{N-1}\tilde{u}_j(t)dt, \tag{A3b}$$

$$d\tilde{u}_j(t) = [-\eta_j v_j - v_j\tilde{u}_j(t)]dt + \sqrt{2v_j\eta_j k_B T}\,d\tilde{W}_j(t). \tag{A3c}$$

Here $\tilde{\mathbf{W}}(t) := \{\tilde{W}_0(t), \ldots, \tilde{W}_{N-1}(t)\}^*$ is standard (zero-mean) Brownian motion under Q. Superscript * is the transposition operator. The state vector is denoted as $\mathbf{X}(t) := \{x(t)\ v(t)\ u_0(t)\ \ldots\ u_{N-1}(t)\}^*$. For notational convenience, the unforced drift vector is denoted as

$$\mathbf{b}(\mathbf{X}_t,t) = \left\{ v_t,\ (-\omega^2/m)x_t + (1/m)\sum_{i=0}^{N-1}u_j(t),\ (-\eta_0 v_0(t) - v_0 u_0(t)), \ldots, [-\eta_{N-1}v_{N-1}(t) - v_{N-1}u_{N-1}(t)] \right\}^*.$$

The forcing drift vector (containing the sinusoidal force as the only nonzero component) is denoted as $\mathbf{h}(t) = \{h_0(t), \ldots, h_{N+1}(t)\}^*$, where $h_1(t) = h_2(t) = 0$ and $h_{j+2}(t) := (A/\sqrt{N^2 2v_j\eta_j k_B T})[\omega_f\cos(\omega_f t) + v_j\sin(\omega_f t)]$, $j = 0,\ldots,N-1$.

In matrix form Eqs. (A3a)–(A3c) may be written as

$$d\mathbf{X}_t = \mathbf{b}(\mathbf{X}_t,t)dt + \mathbf{f}d\tilde{\mathbf{W}}_t, \tag{A4}$$

where $\mathbf{f}$ is a suitably zero-padded rectangular noise intensity (diffusion) matrix of dimension $(N+2)N$ with its only nonzero entries being given by the set

$$\{\mathbf{f}_{i+2,i} : i = 1,...,N\} = \{\sqrt{2v_0\eta_0 k_B T},...,\sqrt{2v_{N-1}\eta_{N-1}k_B T}\}.$$

We are interested in arriving at a weak solution, under original measure P, of $\phi_t(\mathbf{X}) := \phi(\mathbf{X}_t)$, ϕ being any twice differentiable (scalar or vector-valued) function of $\mathbf{X}_t$ [e.g., $\phi_t(\mathbf{X}) = x_t^2$]. Using the system of equations (A3a)–(A3c) under Q, the required solution (under P) may be arrived at by applying the generalized Bayes' formula $E_p(\phi_t) = E_Q(\phi_t\Lambda_t|\mathcal{F}_t^W)/E_Q(\Lambda_t|\mathcal{F}_t^W)$. Here Λ_t denotes the Q-valued Radon-Nikodym derivative dP/dQ associated with the change of measures [36,37], which in this case is given by

$$\Lambda_t = \prod_{j=0}^{N-1}\Lambda_{j,t},$$

where $\Lambda_{j,t} = \exp[\int_0^t h_{j+2}(t)d\tilde{W}_j(t) - \frac{1}{2}\int_0^t h_{j+2}^2(t)dt]$.

In arriving at an explicit evolution equation for the expectation (e.g., the MSD), we start with the stochastic integration by parts formula:

$$d[\phi_t(\mathbf{X})\Lambda_t] = d\phi_t(\mathbf{X})\Lambda_t + \phi_t(\mathbf{X})d\Lambda_t + d\langle\phi_t(\mathbf{X}),\Lambda_t\rangle. \tag{A5}$$

$\langle\cdot,\cdot\rangle$ is the notation for quadratic covariation [38]. We thus have

$$\begin{aligned} d[\phi_t(\mathbf{X})\Lambda_t] &= \Lambda_t\phi_t'(\mathbf{X})^T d\mathbf{X}_t + \frac{1}{2}\Lambda_t\langle d\mathbf{X}_t, \phi_t''(\mathbf{X})d\mathbf{X}_t\rangle + \phi_t(\mathbf{X})\Lambda_t[\mathbf{h}_t(3:N+2)]^* d\tilde{\mathbf{W}}_t + d\langle\phi_t(\mathbf{X}),\Lambda_t\rangle \Rightarrow d[\phi_t(\mathbf{X})\Lambda_t] \\ &= \Lambda_t\Bigg\{[\phi_t'(\mathbf{X})]^*[\mathbf{b}(\mathbf{X}_t,t)dt + \mathbf{f}d\tilde{\mathbf{W}}_t] + \frac{1}{2}\sum_{j,k=1}^{N+2}\sum_{l=1}^{N}\left(\frac{\partial^2\phi}{\partial\mathbf{X}^j\partial\mathbf{X}^k}\right)_t \mathbf{f}^{jl}\mathbf{f}^{kl}dt + \phi_t(\mathbf{X})\,[\mathbf{h}_t\,(3:N+2)]^*\,d\tilde{\mathbf{W}}_t \\ &\quad + \sum_{k=1}^{N+2}\left(\frac{\partial\phi}{\partial\mathbf{X}^k}\right)_t \mathbf{f}_k\mathbf{h}_t(3:N+2)dt\Bigg\}, \end{aligned} \tag{A6}$$

where $\mathbf{h}_t(3:N+2)$ is the N-dimensional vector obtained by removing the first two entries from the vector $\mathbf{h}_t$. For notational convenience, we defined $\mathbf{f}_k$ to be the kth row of the matrix $\mathbf{f}$. Equation (A5) may be written in the integral form as

$$\phi_t(\mathbf{X})\Lambda_t = \phi_0(\mathbf{X})\Lambda_0 + \int_0^t \Lambda_s \Bigg\{ [\phi_s'(\mathbf{X})]^* [\mathbf{b}(\mathbf{X}_s,s)ds + \mathbf{f}d\tilde{\mathbf{W}}_s] + \frac{1}{2}\sum_{j,k=1}^{N+2}\sum_{l=1}^{N}\left(\frac{\partial^2\phi}{\partial\mathbf{X}^j\partial\mathbf{X}^k}\right)_s \mathbf{f}^{jl}\mathbf{f}^{kl}ds + \phi_s(\mathbf{X})[\mathbf{h}_s(3:N+2)]^* d\tilde{\mathbf{W}}_s$$
$$+ \sum_{k=1}^{N+2}\left(\frac{\partial\phi}{\partial\mathbf{X}^k}\right)_s \mathbf{f}_k\mathbf{h}_s(3:N+2)ds \Bigg\}. \tag{A7}$$

Now, it is noted that taking the conditional expectation under Q with respect to $\mathcal{F}_t^W$ is equivalent to "projecting" on the error information generated by $\mathbf{W}_s, s \leqslant t$, and thus enabling a correction to the required expectation, such as the MSD, for such errors. The statistical error information contained in $\mathcal{F}_t^W$ may importantly include any modeling errors in converting the original GLE (1a) to its Markovian representation [e.g., those in the finite sum representations of $\xi(t)$ and $\eta(t-s)$]. Upon taking this conditional expectation, Eq. (A7) reduces to

$$E_Q\left[\phi_t(\mathbf{X})\Lambda_t \middle| \mathcal{F}_t^W\right] = E_Q\left[\phi_0(\mathbf{X})\Lambda_0 \middle| \mathcal{F}_t^W\right] + \int_0^t E_Q\left\{\Lambda_s[\phi_s'(\mathbf{X})]^*\mathbf{b}(\mathbf{X}_s,s)\middle|\mathcal{F}_s^W\right\}ds$$
$$+ \frac{1}{2}\int_0^t E_Q\left[\Lambda_s\sum_{j,k=1}^{N+2}\sum_{l=1}^{N}\left(\frac{\partial^2\phi}{\partial\mathbf{X}^j\partial\mathbf{X}^k}\right)_s \mathbf{f}^{jl}\mathbf{f}^{kl}\middle|\mathcal{F}_s^W\right]ds$$
$$+ \int_0^t E_Q\left[\Lambda_s\sum_{k=1}^{N+2}\left(\frac{\partial\phi}{\partial\mathbf{X}^k}\right)_s \mathbf{f}_k\mathbf{h}_s\,(3:N+2)\,\middle|\mathcal{F}_s^W\right]ds + \int_0^t E_Q\left\{\Lambda_s\phi_s(\mathbf{X})\,[\mathbf{h}_s\,(3:N+2)]^*\,\middle|\mathcal{F}_s^W\right\}d\tilde{\mathbf{W}}_s$$
$$+ \int_0^t E_Q\left\{\Lambda_s[\phi_s'(\mathbf{X})]^*\mathbf{f}\middle|\mathcal{F}_s^W\right\}d\tilde{\mathbf{W}}_s. \tag{A8}$$

Note that the conditional expectation above is measurable with respect to $\mathcal{F}_t^W$ and hence is itself a stochastic process. Defining $\sigma_t(\cdot) := \mathrm{E}_{\mathbf{Q}}[\cdot\,\Lambda_t|\mathcal{F}_t^W]$, we rewrite the above equation in a more convenient form:

$$\sigma_t(\phi) = \sigma_0(\phi) + \int_0^t \sigma_s\{[\phi_s'(\mathbf{X})]^*\mathbf{b}(\mathbf{X}_s,s)\}ds$$
$$+ \frac{1}{2}\int_0^t \sigma_s\left[\sum_{j,k=1}^{N+2}\sum_{l=1}^{N}\left(\frac{\partial^2\phi}{\partial\mathbf{X}^j\partial\mathbf{X}^k}\right)_s \mathbf{f}^{jl}\mathbf{f}^{kl}\right]ds + \int_0^t \sigma_s\left[\sum_{k=1}^{N+2}\left(\frac{\partial\phi}{\partial\mathbf{X}^k}\right)_s \mathbf{f}_k\mathbf{h}_s\,(3:N+2)\right]ds$$
$$+ \int_0^t \sigma_s\{\phi_s(\mathbf{X})\,[\mathbf{h}_s\,(3:N+2)]^*\}d\tilde{\mathbf{W}}_s + \int_0^t \sigma_s\{[\phi_s'(\mathbf{X})]^*\mathbf{f}\}d\tilde{\mathbf{W}}_s. \tag{A9}$$

Since our original system evolution is under P, define $\pi_t(\phi) = E_P(\phi)$ so that we have $\pi_t(\phi) = \sigma_t(\phi)/\sigma_t(1)$, where $\sigma_t(1) = \mathrm{E}_{\mathbf{Q}}[\Lambda_t|\mathcal{F}_t^W]$ may be looked upon as a normalization factor and can be expanded as

$$\sigma_t(1) = \sigma_{t_{i-1}}(1) + \int_0^t \sigma_s\{[\mathbf{h}_s(3:N+2)]^*\}d\tilde{\mathbf{W}}_s. \tag{A10}$$

Note that $\sigma_t(1)$ is an exponential martingale [38] with respect to $\mathcal{F}_t^W$. In estimating the normalized conditional expectation $\pi_t(\phi) = \sigma_t(\phi)/\sigma_t(1)$, we use Ito's formula:

$$d\pi_t(\phi) = d\left(\frac{\sigma_t(\phi)}{\sigma_t(1)}\right) = d\sigma_t(\phi)\frac{1}{\sigma_t(1)} + \sigma_t(\phi)d\left(\frac{1}{\sigma_t(1)}\right) + d\left\langle\sigma_t(\phi),\frac{1}{\sigma_t(1)}\right\rangle_t, \tag{A11}$$

where

$$d\sigma_t(\phi) = \sigma_t\{[\phi_t'(\mathbf{X})]^*\mathbf{b}(\mathbf{X}_t,t)\}dt + \frac{1}{2}\sigma_t\left[\sum_{j,k=1}^{N+2}\sum_{l=1}^{N}\left(\frac{\partial^2\phi}{\partial\mathbf{X}^j\partial\mathbf{X}^k}\right)_t \mathbf{f}^{jl}\mathbf{f}^{kl}\right]dt + \sigma_t\left[\sum_{k=1}^{N+2}\left(\frac{\partial\phi}{\partial\mathbf{X}^k}\right)_s \mathbf{f}_k\mathbf{h}_t\,(3:N+2)\right]dt$$
$$+ \sigma_t\{\phi_t(\mathbf{X})[\mathbf{h}_t(3:N+2)]^*\}d\tilde{\mathbf{W}}_t + \sigma_t\{[\phi_t'(\mathbf{X})]^*\mathbf{f}\}d\tilde{\mathbf{W}}_t$$

and

$$d\left(\frac{1}{\sigma_t(1)}\right) = -\frac{1}{\sigma_t(1)^2}\sigma_t\{[\mathbf{h}_t\,(3:N+2)]^*\}d\tilde{\mathbf{W}}_t + \frac{1}{\sigma_t(1)^3}\sigma_t\{[\mathbf{h}_t\,(3:N+2)]^*\}\sigma_t\,\{[\mathbf{h}_t\,(3:N+2)]\}\,dt$$
$$= -\frac{1}{\sigma_t(1)}\pi_t\{[\mathbf{h}_t\,(3:N+2)]^*\}d\tilde{\mathbf{W}}_t + \frac{1}{\sigma_t(1)}\pi_t\{[\mathbf{h}_t\,(3:N+2)]^*\}\pi_t\,\{[\mathbf{h}_t\,(3:N+2)]\}\,dt.$$

We can thus write

$$d\pi_t(\phi) = d\left(\frac{\sigma_t(\phi)}{\sigma_t(1)}\right) = \pi_t\{[\phi_t'(\mathbf{X})]^*\mathbf{b}(\mathbf{X}_t,t)\}dt + \frac{1}{2}\pi_t\left[\sum_{j,k=1}^{N+2}\sum_{l=1}^{N}\left(\frac{\partial^2\phi}{\partial\mathbf{X}^j\partial\mathbf{X}^k}\right)_t\mathbf{f}^{jl}\mathbf{f}^{kl}\right]dt + \pi_t\{[\phi_t'(\mathbf{X})]^*\mathbf{f}\}d\tilde{\mathbf{W}}_t$$
$$+ \pi_t\{\phi_t(\mathbf{X})\,[\mathbf{h}_t\,(3:N+2)]^*\}d\tilde{\mathbf{W}}_t - \pi_t\,(\phi)\,\pi_t\{[\mathbf{h}_t\,(3:N+2)]^*\}d\tilde{\mathbf{W}}_t$$
$$- (\pi_t\{\phi_t(\mathbf{X})\,[\mathbf{h}_t\,(3:N+2)]^*\}d\tilde{\mathbf{W}}_t)\pi_t\,\{[\mathbf{h}_t\,(3:N+2)]\}$$
$$+ \pi_t\left[\sum_{k=1}^{N+2}\left(\frac{\partial\phi}{\partial\mathbf{X}^k}\right)_s\mathbf{f}_k\mathbf{h}_t\,(3:N+2)\right]dt + \pi_t\,(\phi)\,\pi_t\{[\mathbf{h}_t\,(3:N+2)]^*\}\pi_t\,\{[\mathbf{h}_t\,(3:N+2)]\}\,dt$$
$$- \{\pi_t[(\phi_t'(\mathbf{X}))^*\mathbf{f}]\}\pi_t\,\{[\mathbf{h}_t(3:N+2)]\}\,dt. \tag{A12}$$

As noted before, $\pi_t(\phi)$ is a stochastic process. However, since $\mathbf{h}_t$ is a deterministic function, $E_P[\pi_t(\mathbf{h}_t)] = \mathbf{h}_t$ using which Eq. (A12) may be simplified as

$$E_P\,[d\pi_t(\phi)] = E_P\left[d\left(\frac{\sigma_t(\phi)}{\sigma_t(1)}\right)\right] = E_P(\pi_t\{[\phi_t'(\mathbf{X})]^*\mathbf{b}(\mathbf{X}_t,t)\})dt + \frac{1}{2}E_P\left\{\pi_t\left[\sum_{j,k=1}^{N+2}\sum_{l=1}^{N}\left(\frac{\partial^2\phi}{\partial\mathbf{X}^j\partial\mathbf{X}^k}\right)_t\mathbf{f}^{jl}\mathbf{f}^{kl}\right]\right\}dt$$
$$+ E_P(\pi_t\{[\phi_t'(\mathbf{X})]^*\mathbf{f}\}d\tilde{\mathbf{W}}_t) - E_P(\{\pi_t(\phi)[\mathbf{h}_t(3:N+2)]^*d\tilde{\mathbf{W}}_t\})[\mathbf{h}_t(3:N+2)]$$
$$+ E_P\,[\pi_t\,(\phi)]\,[\mathbf{h}_t\,(3:N+2)]^*\,[\mathbf{h}_t\,(3:N+2)]\,dt.$$

In the integral form, one obtains

$$E_P\,[\pi_t(\phi)] = E_P\,[\pi_0(\phi)] + E_P\left(\int_0^t\pi_s\{[\phi_s'(\mathbf{X})]^*\mathbf{b}(\mathbf{X}_s,s)\}ds\right) + E_P\left\{\int_0^t\frac{1}{2}\pi_s\left[\sum_{j,k=1}^{N+2}\sum_{l=1}^{N}\left(\frac{\partial^2\phi}{\partial\mathbf{X}^j\partial\mathbf{X}^k}\right)_s\mathbf{f}^{jl}\mathbf{f}^{kl}\right]dt\right\}$$
$$+ E_P\left(\int_0^t\pi_s\{[\phi_s'(\mathbf{X})]^*\mathbf{f}\}d\tilde{\mathbf{W}}_s\right) - E_P\left(\int_0^t\{\pi_s\,(\phi)\,[\mathbf{h}_s\,(3:N+2)]^*\,d\tilde{\mathbf{W}}_s\}\,[\mathbf{h}_s\,(3:N+2)]\right)$$
$$+ E_P\left\{\int_0^t\pi_s\,(\phi)\,[\mathbf{h}_s\,(3:N+2)]^*\,[\mathbf{h}_s\,(3:N+2)]\,ds\right\}. \tag{A13}$$

Ito integrals in Eq. (A13) are zero-mean Brownian motions. Hence by taking expectation on both sides of Eq. (A13) it may be further modified as

$$E_P\,[\pi_t(\phi)] = E_P\,[\pi_0(\phi)] + \int_0^t E_P(\pi_s\{[\phi_s'(\mathbf{X})]^*\mathbf{b}(\mathbf{X}_s,s)\})ds + \int_0^t\frac{1}{2}E_P\left\{\pi_s\left[\sum_{j,k=1}^{N+2}\sum_{l=1}^{N}\left(\frac{\partial^2\phi}{\partial\mathbf{X}^j\partial\mathbf{X}^k}\right)_s\mathbf{f}^{jl}\mathbf{f}^{kl}\right]\right\}dt$$
$$+ \int_0^t E_P\,[\pi_s\,(\phi)]\,[\mathbf{h}_s\,(3:N+2)]^*\,[\mathbf{h}_s\,(3:N+2)]\,ds. \tag{A14}$$

In particular, when $\phi(\mathbf{X}_t) = x_t^2$, Eq. (A14) may be used to obtain the following equation for the MSD:

$$E_P[\pi_t(x^2)] = E_P[\pi_0(x^2)] + \int_0^t E_P\{\pi_s[(2x)^*\mathbf{b}(\mathbf{X}_s,s)]\}ds + \int_0^t \frac{1}{2}E_P\left\{\pi_s\left[\sum_{j,k=1}^{N+2}\sum_{l=1}^{N}\left(\frac{\partial^2(x^2)}{\partial\mathbf{X}^j\partial\mathbf{X}^k}\right)_s \mathbf{f}^{jl}\mathbf{f}^{kl}\right]\right\}ds$$
$$+ \int_0^t E_P[\pi_s(x^2)]\,[\mathbf{h}_s\,(3:N+2)]^*\,[\mathbf{h}_s\,(3:N+2)]\,ds. \tag{A15}$$

From Eq. (A15) we see that the forcing contribution through $\int_0^t E_P[\pi_s(x^2)][\mathbf{h}_s(3:N+2)]^*[\mathbf{h}_s(3:N+2)]ds$ is strictly positive.

[1] G. Maret and P. Wolf, Z. Phys. B **65**, 409 (1987).
[2] D. J. Pine, D. A. Weitz, P. M. Chaikin, and E. Herbolzheimer, Phys. Rev. Lett. **60**, 1134 (1988).
[3] R. Pecora, *Dynamic Light Scattering: Applications of Photon Correlation Spectroscopy* (Springer, New York, 1985).
[4] T. Gisler and D. Weitz, Curr. Opin. Colloid Interface Sci. **3**, 586 (1998).
[5] D. A. Boas, L. E. Campbell, and A. G. Yodh, Phys. Rev. Lett. **75**, 1855 (1995).
[6] C. Zhou, G. Yu, D. Furuya, J. Greenberg, A. Yodh, and T. Durduran, Opt. Express **14**, 1125 (2006).
[7] M. Heckmeier and G. Maret, Europhys. Lett. **34**, 257 (1996).
[8] S. Skipetrov and I. Meglinskii, J. Exp. Theor. Phys. **86**, 661 (1998).
[9] H. Varma, A. Nandakumaran, and R. Vasu, J. Opt. Soc. Am. A **26**, 1472 (2009).
[10] A. Gibson, J. Hebden, and S. Arridge, Phys. Med. Biol. **50**, R1 (2005).
[11] W. Leutz and G. Maret, Phys. B: Condens. Matter **204**, 14 (1995).
[12] M. Kempe, M. Larionov, D. Zaslavsky, and A. Genack, J. Opt. Soc. Am. A **14**, 1151 (1997).
[13] C. Kim, L. Wang, I. Vellekoop, A. Mosk, T. Wu, J. Qu, M. Xu, W. Cottrell, J. Wilson, T. Foster *et al.*, Opt. Lett. **32**, 2285 (2007).
[14] H. Varma, K. Mohanan, N. Hyvönen, A. Nandakumaran, and R. Vasu, J. Opt. Soc. Am. A **28**, 2322 (2011).
[15] M. Priestley, J. Sound Vib. **6**, 86 (1967).
[16] R. N. Zia and J. F. Brady, J. Fluid. Mech. **658**, 188 (2010).
[17] R. Mankin, K. Laas, and A. Sauga, Phys. Rev. E **83**, 061131 (2011).
[18] I. Goychuk, Phys. Rev. E **80**, 046125 (2009).
[19] A. Gemant, J. Appl. Phys. **7**, 311 (1936).
[20] R. Kubo, Rep. Prog. Phys. **29**, 255 (1966).
[21] V. Kharchenko and I. Goychuk, New J. Phys. **14**, 043042 (2012).
[22] Technical note No. TPHO9001E04, Hamamatsu Photonics K. K, Electron Tube division, Japan, 2005 (unpublished).
[23] K. Schätzel, M. Drewel, and S. Stimac, J. Mod. Opt. **35**, 711 (1988).
[24] D. Magatti and F. Ferri, Appl. Opt. **40**, 4011 (2001).
[25] C. Bohren and D. Huffman, *Absorption and Scattering of Light by Small Particles* (Wiley-VCH, Weinheim, 2008).
[26] F. Scheffold, S. E. Skipetrov, S. Romer, and P. Schurtenberger, Phys. Rev. E **63**, 061404 (2001).
[27] F. Scheffold, S. Romer, F. Cardinaux, H. Bissig, A. Stradner, L. Rojas-Ochoa, V. Trappe, C. Urban, S. Skipetrov, L. Cipelletti *et al.*, Trends Colloid Interface Sci. XVI **123**, 141 (2004).
[28] J. Harden and V. Viasnoff, Curr. Opin. Colloid Interface Sci. **6**, 438 (2001).
[29] R. Bandyopadhyay, A. Gittings, S. Suh, P. Dixon, and D. Durian, Rev. Sci. Instrum. **76**, 093110 (2005).
[30] N. Menon and D. J. Durian, Science **275**, 1920 (1997).
[31] T. Mason, Rheol. Acta **39**, 371 (2000).
[32] B. R. Dasgupta and D. A. Weitz, Phys. Rev. E **71**, 021504 (2005).
[33] B. R. Dasgupta, S.-Y. Tee, J. C. Crocker, B. J. Frisken, and D. A. Weitz, Phys. Rev. E **65**, 051505 (2002).
[34] C. Devi, R. Chandran, R. Vasu, and A. Sood, J. Biomed. Opt. **12**, 034035 (2007).
[35] R. Mankin and A. Rekker, Phys. Rev. E **81**, 041122 (2010).
[36] T. Raveendran, S. Sarkar, D. Roy, and R. M. Vasu, Inverse Probl. **29**, 065002 (2013).
[37] N. Saha and D. Roy, J. Appl. Mech. **74**, 885 (2007).
[38] B. Øksendal, *Stochastic Differential Equations: An Introduction with Applications*, 6th ed. (Springer, Berlin, 2003).